JVI Journals.ASM.org

The Structure and Host Entry of an Invertebrate Parvovirus

Geng Meng,[a] Xinzheng Zhang,[a] Pavel Plevka,[a]* Qian Yu,[b] Peter Tijssen,[b] Michael G. Rossmann[a]

Department of Biological Sciences, Purdue University, West Lafayette, Indiana, USA[a]; INRS-Institut Armand-Frappier, Université du Québec, Laval, Québec, Canada[b]

The 3.5-Å resolution X-ray crystal structure of mature cricket parvovirus (*Acheta domesticus* densovirus [*Ad*DNV]) has been determined. Structural comparisons show that vertebrate and invertebrate parvoviruses have evolved independently, although there are common structural features among all parvovirus capsid proteins. It was shown that raising the temperature of the *Ad*DNV particles caused a loss of their genomes. The structure of these emptied particles was determined by cryo-electron microscopy to 5.5-Å resolution, and the capsid structure was found to be the same as that for the full, mature virus except for the absence of the three ordered nucleotides observed in the crystal structure. The viral protein 1 (VP1) amino termini could be externalized without significant damage to the capsid. *In vitro*, this externalization of the VP1 amino termini is accompanied by the release of the viral genome.

Parvoviruses are small (~250- to 300-Å-diameter), single-stranded DNA (ssDNA), icosahedral (T=1), nonenveloped viruses whose genomes are approximately 5 kb long (1). The *Parvoviridae* family has been subdivided into viruses that infect vertebrates (*Parvovirinae*) and those that infect invertebrates (*Densovirinae*) (2). Parvoviruses replicate in dividing cells such as in tissues from insect larvae and fetuses. Densoviruses are highly pathogenic, and those that use insect hosts usually kill 90% of the larvae within a few days (2). Densoviruses pose a threat to commercial invertebrates such as shrimp (3), silkworms (4), and crickets (5, 6). Some highly pathogenic densoviruses are potential selective pesticides for vectors that transmit mosquito-borne diseases (7). *Parvovirinae* generally have three types of proteins (VP1, VP2, and VP3) in their capsids (8), whereas *Densovirinae* generally have four types of proteins (VP1 to VP4) in their capsids (2). In densoviruses there are 200 additional amino acids in VP1 at the N terminus. These different proteins result from different initiation sites for translation of the capsid gene and from posttranslational modification of their N termini (8). Generally, each of the 60 subunits within a capsid has the same amino acid sequence and is structurally the same, except that the different proteins start at different amino acids. The VP2s of some densoviruses are unique among VP2s of parvoviruses since they are not completely contained within corresponding VP1s (Fig. 1A).

Parvoviruses enter cells by dynamin-dependent receptor-mediated endocytosis and escape the endosome by the phospholipase (PLA2) activity within the amino-terminal domain of VP1 (9–13). Although there is often less than 5% amino acid identity among the structural proteins of parvoviruses, the sequence of the PLA2 N-terminal domain of VP1 has more than 30% amino acid identity (Fig. 1A and B). The PLA2 domain is not exposed in assembled, full parvoviruses such as minute virus of mice (MVM) (13) and human parvovirus B19 (14), and it therefore has to be exposed during endocytosis (9, 11, 13–15). However, the mechanism by which the VP1 amino-terminal PLA2 domain is exposed has not been elucidated in detail (16).

The structures of six autonomous vertebrate parvoviruses (canine parvovirus [CPV] [17], feline parvovirus [FPV]) [18], porcine parvovirus [PPV] [19], MVM [20], H-1 parvovirus [H-1PV] [21], and human parvovirus B19 [22]) and three invertebrate parvoviruses (*Galleria mellonella* densovirus [*Gm*DNV] [23], *Bombyx mori* densovirus [*Bm*DNV] [24], and *Penaeus stylirostris* densovirus [*Pst*DNV] [25]) have been determined (Table 1). Furthermore, extensive studies have been made of the human adeno-associated dependoviruses (26, 27). The structures of these parvoviruses consist of 60 structurally equivalent capsid proteins assembled with icosahedral symmetry. Each capsid protein has a "jelly roll" fold, a motif that is common to many viruses, including the nonenveloped RNA picornaviruses (28) and small RNA plant viruses (29) as well as larger double-stranded DNA (dsDNA) adenoviruses (30), the enveloped bacteriophage PRD1 (31), the fungal virus *Paramecium bursaria* chlorella virus 1 (PBCV-1) (32), vaccinia virus (33), and probably also mimivirus (34). The jelly roll fold is a β-barrel consisting of two opposed antiparallel β-sheets with adjacent-strand BIDG and CHEF, where the strands along the polypeptide chain are named A and B to H. The interior of the barrel is exceedingly hydrophobic.

Parvoviruses have a channel along the 5-fold axes formed by five symmetry-related DE loops (the "DE" loop is between the β-strands D and E). Residues lining the channel are mostly hydrophobic and guide the externalization of a conserved glycine-rich sequence near the amino ends of the VPs (35–37). The loops connecting the β-strands of the jelly roll fold are usually exceptionally large in parvoviruses compared with the loops in picornaviruses (28, 38) and form the exterior of the virus and intersubunit contacts (Fig. 1C). These loops are more variable in sequence than the core jelly roll structure.

Here, we describe the crystal structure of mature virions of cricket parvovirus (*Acheta domesticus* densovirus [*Ad*DNV]) at 3.5-Å resolution and the cryo-electron microscopic (cryoEM) structure of the emptied virus at 5.5-Å resolution. We also report on the externalization of the VP1 N-terminal region and subsequent genome release by an increase in temperature.

Received 3 July 2013 **Accepted** 3 September 2013

Published ahead of print 11 September 2013

Address correspondence to Michael G. Rossmann, mr@purdue.edu.

* Present address: Pavel Plevka, CEITEC, Masaryk University, Brno, Czech Republic.

doi:10.1128/JVI.01822-13

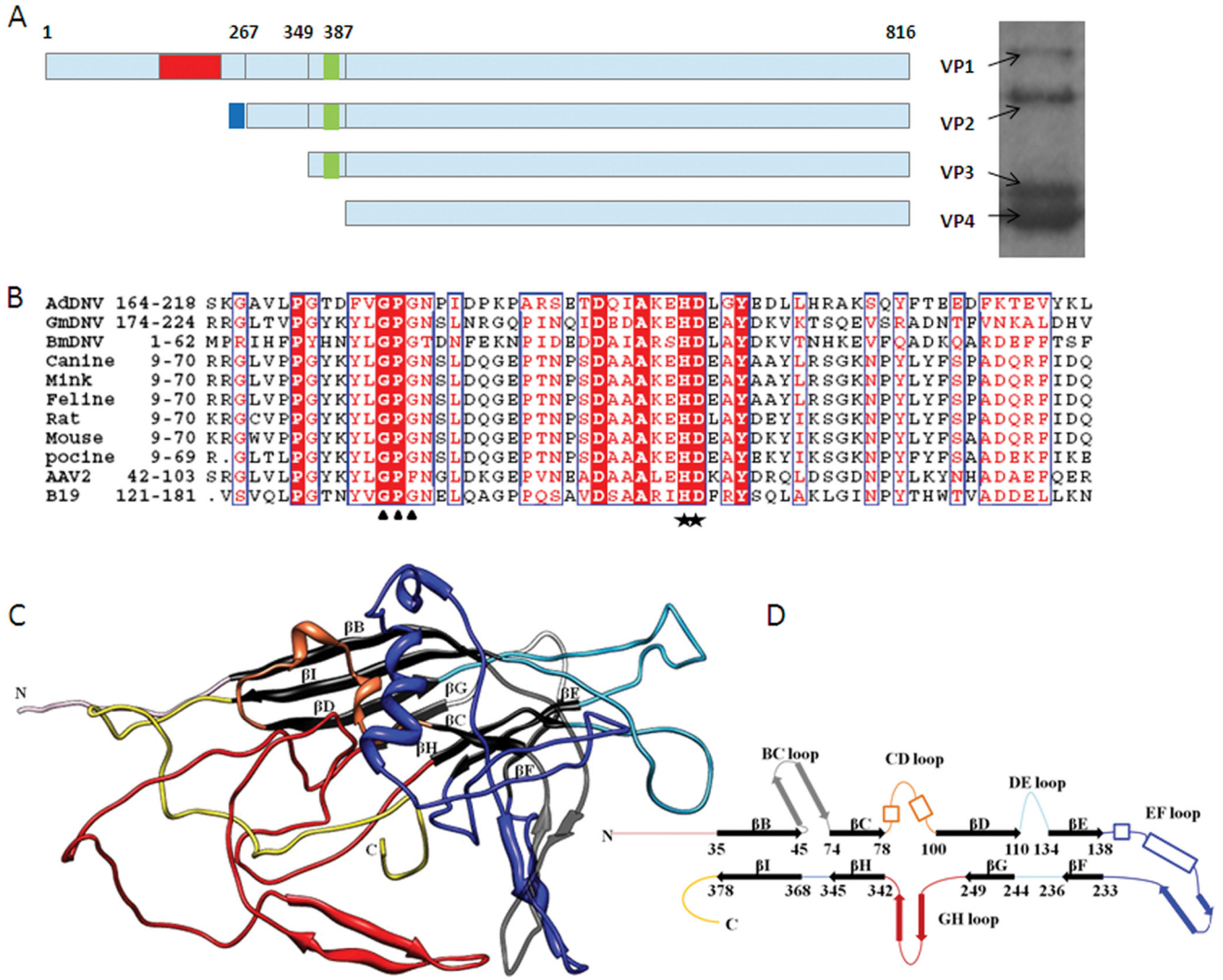

FIG 1 Structure of the *Ad*DNV capsid protein. (A) Left, capsid protein organization. Red area, PLA2 domain; green area, glycine-rich region; blue area, extra sequence at the N termini of VP2. Right, SDS-polyacrylamide gel of the *Ad*DNV full particles. (B) Alignment of PLA2 sequences in VP1s of various parvoviruses, including *Ad*DNV, *Gm*DNV, *Bm*DNV, CPV, mink parvovirus, FDV, rat parvovirus, mouse parvovirus, PPV, AAV2, and B19. The stars indicate the His-Asp catalytic site, and the triangles locate the Ca^{2+}-binding site. (C) Three-dimensional structure of *Ad*DNV capsid protein, showing the core jelly roll in black. The surface loops connecting the strands of the core jelly roll are colored as follows: BC loop, gray; CD loop, orange; DE loop, sky blue; EF loop, dark blue; and GH loop, red. (D) Diagrammatic representation of the capsid protein structure (heavy lines represent β-strands) (color coding is the same as in panel C).

MATERIALS AND METHODS

Virus purification and preparation of the emptied virus particles. The original virus was isolated from infected crickets (5). Further purification was achieved using CsCl equilibrium density gradient centrifugation. Of the two bands with different densities, the lower band contained the full particles and represented 99% of all the particles. The upper band contained empty particles assembled mainly from VP4. The two bands were separately transferred into Tris-buffered saline (TBS) (10 mM Tris-Cl, 100 mM NaCl, 1 mM CaCl, and 1 mM MgCl at pH 7.5) for further usage. Aliquots of the full virus particles were incubated at 26, 37, 45, 55, 65, 75, and 100°C for 1 h. The heat-treated emptied particles were frozen on holey carbon (Quantifoil) EM grids and checked by cryoEM. The numbers of full, empty, and broken particles were counted by eye (Fig. 2) and averaged over three holes on two different EM grids. Each hole had roughly 100 particles.

Determination of the crystal structure of the full virus particle. Crystals of the full particles were obtained by hanging-drop vapor diffusion in the presence of 20% polyethylene glycol (PEG) 400 and 100 mM $MgCl_2$ at 16°C. Further optimization of the crystallization conditions produced crystals of up to 0.5 mm in length. Crystals were soaked for at least 20 min in the presence of 20% glycerol cryoprotectant prior to freezing.

X-ray diffraction data were collected at 100 K at the Advanced Photon Source (APS) beamline 23ID (Table 2). Diffraction data from about 20 crystals were indexed and merged, using the HKL2000 computer program (39) to generate the final 3.5-Å resolution data set. The space group was $P4_22_12$ with $a = 412.67$ Å and $c = 278.80$ Å. The Matthews coefficient was 3.64 $Å^3$/Da, assuming half a virus particle per crystallographic asymmetric unit. Thus, the virus was located on a crystallographic 2-fold axis. A self-rotation function, calculated with the GLRF program (40) using 8- to 3.5-Å resolution data, gave the accurate orientation of the particle about the crystallographic 2-fold axis. This showed that one of the icosahedral 2-fold axes of the virus was roughly parallel to the 4_2 crystallographic axis, with a 1.6° rotation away from being exactly parallel. As a consequence, the position of the particle along the crystallographic 2-fold axis could be

TABLE 1 Structural studies of autonomous parvoviruses

Virus	Description of particle	Structural protein(s) in particles	Resolution (Å)	Icosahedral ordered genome structure (bp)	PDB code (reference)
Vertebrate parvoviruses					
Canine parvovirus	Full virus	VP1, VP2, VP3	2.9	11	4DPV (17)
	Empty particle	VP1, VP2	3.0	None	2CAS (56)
Feline parvovirus	Empty particle	VP3	3.3	None	1FPV (18)
Porcine parvovirus	Virus-like particle	VP2	3.5	None	1K3V (19)
Human parvovirus B19	Virus-like particle	VP2	3.5	None	1S58 (22)
Minute virus of mice	Full virus	VP1, VP2, VP3	3.5	11	1MVM (20)
Rat H-1 parvovirus	Full virus	VP1, VP2, VP3	2.7	10	4G0R (21)
	Empty particle	Unknown	3.2	None	4GBT
Invertebrate parvoviruses					
*Gm*DNV	Full virus	VP1, VP2, VP3, VP4	3.7	None	1DNV (23)
*Bm*DNV	Virus-like particle	VP3	3.1	None	3P0S (24)
*Pst*DNV	Virus-like particle	VP4	2.5	None	3N7X (25)
*Ad*DNV	Full virus	VP1, VP2, VP3, VP4	3.5	3	
	Induced emptied particle	VP1, VP2, VP3, VP4	5.5	None	

determined from the big Patterson peak generated by the large number of parallel equal-length vectors.

The structure was determined using the molecular replacement method (41) with the structure of *Gm*DNV (Protein Data Bank [PDB] code 1DNV) (23) as the initial phasing model to 15-Å resolution. The phases were then extended to 3.5-Å resolution in steps of one reciprocal lattice interval (1/c) at a time. Three cycles of 30-fold noncrystallographic symmetry (NCS) averaging and solvent flattening were performed for each extension step. The averaging and extension processes were performed using the program AVE in the Uppsala Software Factory (42) and FFT, SFALL in CCP4 programs (43). The final overall correlation coefficient between the observed structure amplitudes and the calculated structure factors corresponding to the final averaged and solvent-flattened map was 0.866. The atomic model was built into the 3.5-Å resolution map using COOT (44). The model coordinates were refined with the CNS program (45) while applying NCS constraints and reasonable model restraints, including group temperature factor refinement. No attempt was made to identify water molecules, as the data extended to only 3.5-Å resolution. The structures of the three ordered nucleotides bound to the inside surface of the capsid (see Results and Discussion) were included in

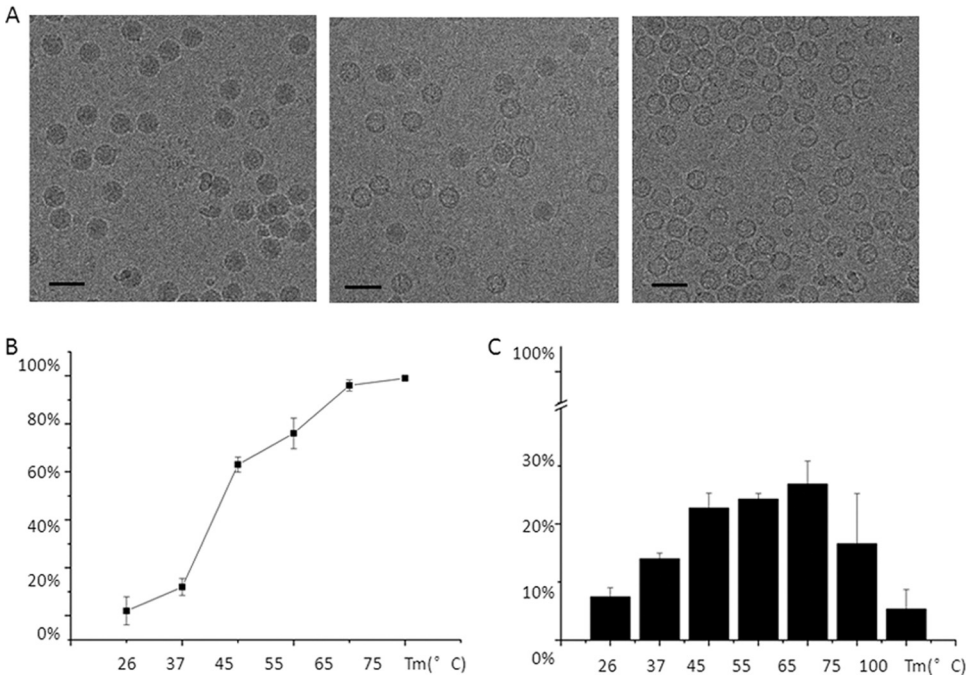

FIG 2 Heat treatment and PLA2 activity of the virus particles. (A) CryoEM micrographs showing the virus after incubation for 1 h at 26°C, 45°C, and 65°C, resulting in only full particles (left), about an equal number of full and emptied particles (middle), and emptied particles (right), respectively. (B) Percentage of emptied particles after incubating full particles at different temperatures. (C) Phospholipase activity as a function of temperature with respect to the PLA2 activity of honey bee PLA2 at 26°C.

TABLE 2 X-ray data collection and structure refinement

Parameter	Value[a]
Data collection parameters	
Wavelength (Å)	1.0715
CCD detector	MAR CCD-325
Exposure time/frame (s)	3
Oscillation angle/frame (°)	0.3
No. of frames collected	300
Data reduction and refinement statistics	
Resolution range (Å)	50–3.5 (3.6–3.5)
Space group	$P4_22_12$
No. of frames used	80
Cell parameters	
a, *b*, *c* (Å)	412.67, 412.67, 278.80
α, β, γ (°)	90, 90, 90
Mosaicity (°)	0.40
No. of observed reflections	1,518,629
No. of unique reflections	236,217 (9,755)
Redundancy	1.2 (1.1)
% Completeness	56 (46.5)
$\langle I\rangle/\langle\sigma(I)\rangle$	4.0 (1.2)
*R*sym $\Sigma h\Sigma j\lvert Ihj-\langle Ih\rangle\rvert/\Sigma\Sigma Ihj$	0.161 (0.565)
Model building and refinement statistics	
Resolution range (Å)	30–3.5 (3.6–3.5)
No. of residues/atoms built	412/3,290
Final *R* factor[b]	0.289
Mean isotropic temp factor (Å2)	18
RMSD bond length (Å)/bond angle (°)	0.0047/1.258
% Residues in most favored/additionally allowed/generously allowed/disallowed regions of the Ramachandran plot[c]	82.5/16.9/0.3/0.3

[a] Values in parentheses refer to the highest-resolution shell.
[b] No R_{free} value was calculated, because the high NCS redundancy interrelates reflections, causing the free reflections to be dependent on all other reflections. As a result, there would be little difference between $R_{working}$ and R_{free}.
[c] Percentage of a total of 360 nonglycine, nonproline residues as defined in the program PROCHECK.

the final stages of refinement. After more than 5 cycles of refinement and model rebuilding, the *R* factor had dropped from 34% to 28.9%. In the presence of the 30-fold NCS redundancy, there will be no significant difference between R_{free} and $R_{working}$.

Detecting the externalized VP1 N termini and their phospholipase A2 activity. Full particles and the heat-treated emptied particles were digested by trypsin at room temperature. About 30 μl of the particle suspension at a concentration of 5 μg/μl was incubated with trypsin for 1 h at 26°C. The trypsin had a final concentration of 1 μg/μl in the mixture. The samples were then checked for VP1 cleavage using a 15% SDS-polyacrylamide gel (Fig. 3).

The PLA2 activities of the full particles and the heat-treated emptied particles were measured at 26°C by a colorimetric assay (sPLA2 assay kit; Cayman Chemical, Ann Arbor, MI), using the 1,2-dithio analog of diheptanoyl phosphatidylcholine (diheptanoyl thio-PC) as the substrate for PLA2. The absorbance at 405 nm was determined every minute for 30 min. Measurements of the PLA2 activity were normalized relative to the activity of 1 ng bee venom PLA2. The activity of the PLA2 in 1.5 μg virus is equivalent to the PLA2 activity in 1 ng bee venom.

CryoEM and three-dimensional structural reconstruction of emptied particles. The optimal condition for obtaining the largest percentage of emptied, unbroken particles was 55C° for 1 h (Fig. 2). Three microliters of the heat-treated emptied particles at a protein concentration of 5 μg/μl

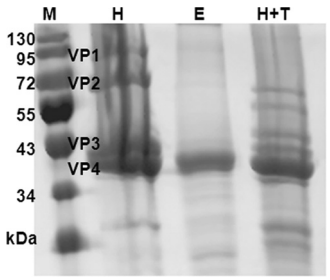

FIG 3 SDS-PAGE of heat-treated *Ad*DNV particles. Lanes: M, protein markers; H, heat-treated emptied *Ad*DNV particles; E, non-heat-treated empty particles among the purified mature *Ad*DNV particles; H+T, further trypsin digestion of the heat-treated emptied *Ad*DNV particles.

was applied to holey grids (Quantifoil) and blotted for 6 s in an FEI Mark 3 Vitrobot chamber at 90% humidity. The grids were then fast-frozen in liquid ethane. Cryo-electron microscopy (CryoEM) images were acquired on an FEI Titan Krios operated at 300 keV. Images were recorded with a 4k × 4k charge-coupled device (CCD) detector. As a control, grids of untreated particles were prepared and viewed in the same way. The assumed magnification of 59,000 was calibrated with respect to a known specimen and was shown to correspond to a pixel separation of 1.51 Å in the image. The electron dose was ~20 $e/Å^2$, and the image was defocused by between ~1.6 and 2.6 μm. About 150 cryoEM micrographs, each showing roughly 100 particles, of the emptied particles were recorded. The defocus and the astigmatism of each micrograph were estimated with the EMAN1 fitctf program (46) and further confirmed with the program ctfit. Image processing and three-dimensional reconstruction were performed using the EMAN suite of programs (47). The final reconstruction was computed using ~15,000 particles out of about 17,000 initial boxed images and was found to have 5.5-Å resolution based on the separate structure determinations of two randomly selected independent sets of images using the Fourier shell correlation threshold of 0.143 (Fig. 4) (48).

Sequence alignment of the PLA2 domain and structural comparisons. The sequence of the *Ad*DNV VP1 N-terminal PLA2 domain (GI 326392953) was aligned with the corresponding sequences of adeno-associated virus 2 (AAV2) (GI 110645923), human parvovirus B19 (GI 169212578), CPV (GI 116646110), MVM (GI 332290), rat parvovirus (GI 410443463), mink parvovirus (GI 425696394), PPV (GI 46404508), *Gm*DNV (GI 23334609), and *Bm*DNV (GI 18025360) using Clustal X (49).

The crystal structure of *Ad*DNV was compared with those of other invertebrate densoviruses, i.e., *Gm*DNV (23) and *Bm*DNV (24), as well as

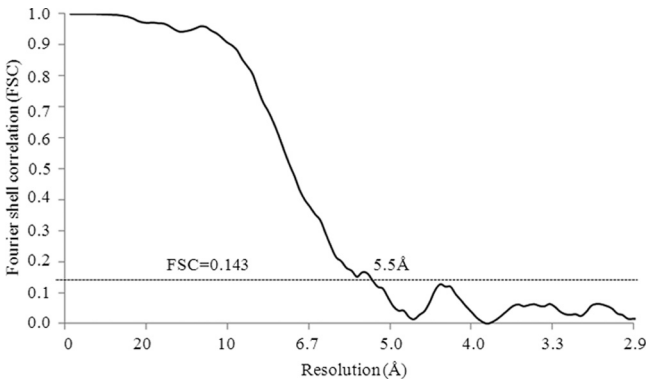

FIG 4 Fourier shell correlation (FSC) based on the independent structure determinations of two randomly selected equally sized sets of images, showing the resolution of the emptied *Ad*DNV particle reconstruction to be ~5.5 Å when the FSC is 0.143.

TABLE 3 Sequence and structural comparisons of *Ad*DNV capsid protein with other autonomous parvovirus capsid proteins

Virus	Sequence identity (%)	RMSD (Å) between Cα atoms	No. of aligned Cα atoms	Total no. of Cα atoms
Canine parvovirus	<5	4.8	261	548
Feline parvovirus	<5	4.9	263	534
Porcine parvovirus	<5	4.9	258	542
Human B19	<5	5.1	260	523
Minute virus of mice	<5	5.0	264	549
*Gm*DNV	30.50	2.1	295	415
*Bm*DNV	<5	3.7	331	412
*Pst*DNV	8.30	4.1	224	299

mammalian autonomous parvoviruses CPV (17), PPV (19), FPV (18), MVM (20), and B19 (22) using the HOMOlogy program (50). These structural comparisons do not include the disordered PLA2 domain, whose positions in the virus are random and therefore cannot be observed in the crystal structure.

Accession numbers. The atomic coordinates of the *Ad*DNV crystal structures have been deposited with the Protein Data Bank (www.pdb.org) (PDB code 4MGU); the cryo-EM maps of the emptied *Ad*DNV particle have been deposited with the Electron Microscopy Data Bank (www.emdatabank.org) (EMDB code EMD-2401).

RESULTS AND DISCUSSION

Crystal structure of the full *Ad*DNV particles. The structure of *Ad*DNV was determined to 3.5-Å resolution. The position of the core jelly roll relative to the icosahedral symmetry axes was essentially the same in *Ad*DNV as in other known parvovirus structures (Table 3 and 4).

The four structural proteins VP1 (88.1 kDa), VP2 (65.3 kDa), VP3 (50.8 kDa), and VP4 (46.9 kDa) are in an approximate 1:11:18:30 proportion in *Ad*DNV full particles based on scanning the gel with Kodak Image Station 2000R and analyzing with software Kodak MI (Fig. 1A). The glycine-rich sequence is present in VP1, VP2, and VP3, but is missing in VP4 (Fig. 1A). It may be significant that, compared with vertebrate parvoviruses, there is therefore only one copy of the PLA2 structure per virion. The polypeptide chain of the capsid protein could be traced from residue 23 of VP4 situated at the base of the 5-fold axis channel to residue 418 at the carboxy terminus (Fig. 1C).

The electron density in this channel ($\sigma = 1.5$) of *Ad*DNV is weak and discontinuous (Fig. 5C), which is similar to the density in the *Gm*DNV 5-fold channel. The glycine-rich motif in *Ad*DNV consists of about 17 residues, 8 of which are glycines, whereas in *Gm*DNV the same motif has 7 glycines and about 16 residues (Fig. 6). The difference of the sequence length may be partly related to the structure of the channel in the different parvoviruses.

The low density in the 5-fold channel suggests that only several of the 12 5-fold channels are occupied, resulting in externalization of the VP amino termini. A similar lack of amino-terminal externalization was observed in *Gm*DNV, the only other known structure of a mature DNV. The structures of silkworm and shrimp densoviruses (Table 1) were self-assembled from recombinantly expressed VP3 and VP4 capsid proteins, respectively. Hence, these structures are missing the glycine-rich sequence. As there is only one VP1 per virion, some of the 5-fold channels must be occupied by VP2 or VP3. However, in the vertebrate parvoviruses CPV (17)

TABLE 4 Superposition of the *Ad*DNV jelly roll core (70 residues) on other invertebrate parvovirus capsid proteins

Virus	RMSD (Å) between Cα atoms
Canine parvovirus	2.0
*Gm*DNV	0.8
*Bm*DNV	1.4
*Pst*DNV	1.6

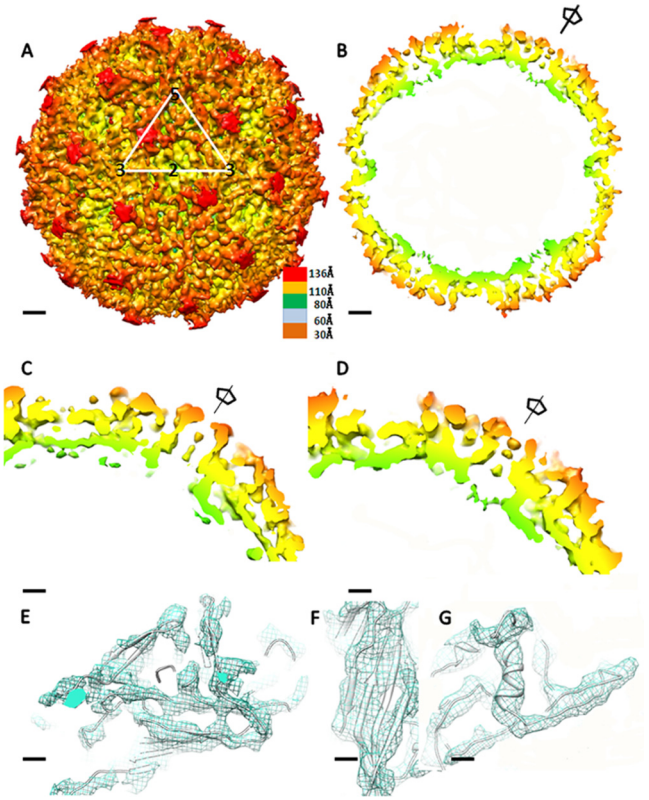

FIG 5 Structure of *Ad*DNV emptied particles. (A) CryoEM reconstruction of emptied particles. Surface features with a triangle showing the limits of one icosahedral asymmetric unit are shown. The scale bars represent 2 nm. (B) Center section of the cryoEM reconstruction. The scale bars represent 2 nm. (C) Enlargement of the 5-fold channel density in the X-ray electron density map. The scale bars represent 1 nm. (D) Enlargement of the 5-fold channel density in the cryoEM density map. The scale bars represent 1 nm. (E, F, and G) Fit of the X-ray structure polypeptide backbone into the cryoEM density for the β-sheets of the jelly roll (scale bars represent 5 Å) (E), the BIDG β-sheet (the scale bars represent 3 Å) (F), and the α-helix located in the EF loop (the scale bars represent 3 Å) (G).

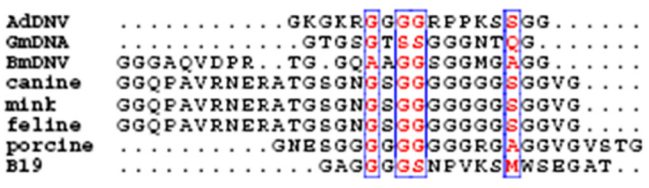

FIG 6 Sequence comparisons of the glycine-rich regions of *Ad*DNV and other autonomous parvovirus, including *Gm*DNV (GI 23334609), *Bm*DNV (GI 18025360), canine parvovirus (CPV) (GI 116646110), mink enteritis virus (MEV) (GI 425696394), feline parvovirus (FPV) (GI 333476), porcine parvovirus (PPV), and human parvovirus (B19) (GI 169212578).

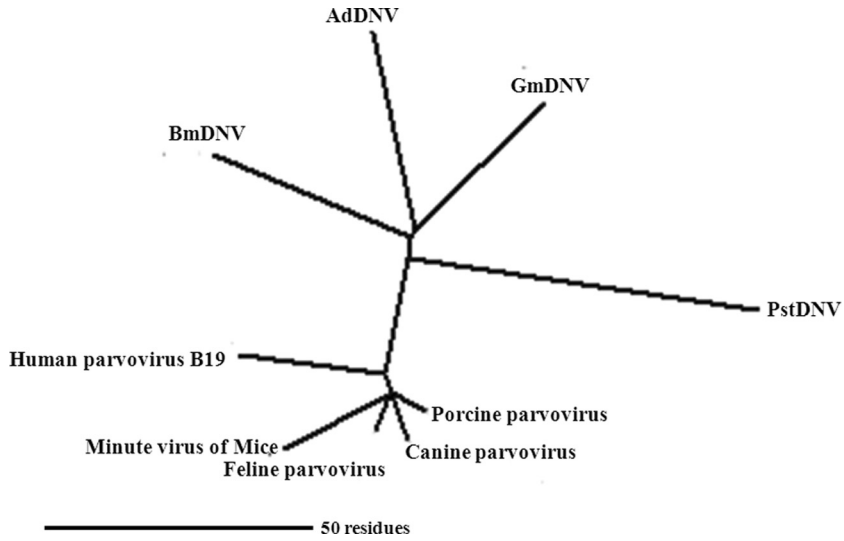

FIG 7 Unrooted phylogenetic tree of different parvoviruses based on the number of inserted residues between β-strands.

and MVM (20), all the 5-fold channels are always fully occupied by the VP amino termini. Furthermore, there is a larger proportion of VP1 subunits per virion in the vertebrate parvoviruses. However, the externalized amino termini are disordered in both the vertebrate and invertebrate parvovirus crystal structures.

Pairwise comparisons of the parvovirus structures were used to determine the number of and root mean square deviation (RMSD) between equivalent Cα atoms (Table 3). The number of inserted amino acids between β-strands was used to calculate a phylogenetic tree using the program MEGA (51) (Fig. 7). This shows a closer relationship among the insect densoviruses (*Ad*DNV, *Gm*DNV, *Pst*DNV, and *Bm*DNV) than between these viruses and vertebrate viruses. Although the capsid proteins of all parvoviruses have common structural features, the capsid proteins of vertebrate and invertebrate parvoviruses must have evolved independently (Fig. 7).

The A β-strand is folded back to run antiparallel to β-strand B in the BIDG sheet in all known vertebrate parvovirus structures (Fig. 1D). In previously determined densovirus structures, including the *Ad*DNV structure reported here, β-strand A is associated with β-strand B in the neighboring, 2-fold related BIDG sheet. Such an exchange of domains between 2-fold-related structures is an example of "domain swapping" (Fig. 1C and D). However, in *Ad*DNV the A β-strand contains three proline residues (Pro24, Pro26, and Pro28) and therefore diminishes the H bonding with the B β-strand of the neighboring subunit.

The channel along the 5-fold icosahedral axes of parvoviruses is formed by the DE loop and is between 16 Å and 18 Å in diameter, measured from atom center to atom center. The conformation of the DE loop is variable among both vertebrate and invertebrate parvoviruses (8). In *Ad*DNV, as also in all other known parvoviruses, there are several hydrophobic amino acids in the DE loop (from 116 Ala to 133 Gln in *Ad*DNV) that interact with the glycine-rich region.

Emptied densovirus particles and phospholipase activity. Most parvoviruses, including densoviruses, assemble *in vivo* both as full infectious particles and as empty particles. However, for *Ad*DNV and presumably also for other densoviruses, the small fraction of particles that are empty in a virus preparation consist of only VP4 (Fig. 3) and are missing the glycine-rich sequence, whereas the dominant infectious virus particles contain all four types of subunits (VP1 to VP4) (Fig. 1A). Therefore, after heat treatment, nearly all the emptied particles that have a full complement of all four VPs must have been full of genome, whereas empty particles containing only VP4 must have been assembled as empty particles. It had been shown that heating parvoviruses to 70°C generated PLA2 activity, suggesting exposure of the VP1 N termini (12, 13). However, it was not clear whether only the VP1 N termini were exposed from intact particles or whether the particles had disassembled. The loss of the genome associated with a presumably transient change in the capsid has some resemblance to the infectious process in picornaviruses (52).

Here we used cryoEM to show that on heating of *Ad*DNV for a defined length of time, the number of emptied particles increased with temperature (Fig. 2A and B). When the temperature was increased beyond 65°C there was also an increase of broken particles. Concomitant with the increase of emptied particles, there was also an increase of PLA2 activity (Fig. 2C). Above about 65°C, the virions disintegrated and had reduced PLA2 activity. Unlike the case for full, infectious *Ad*DNV particles, the VP1 N termini of the heat-treated emptied particles were sensitive to trypsin digestion, whereas the capsids remained intact as determined with

TABLE 5 Results of a six-dimensional search on fitting of the *Ad*DNV capsid protein structure into the 5.5-Å cryoEM density by using the EMfit program (55)[a]

Sumf[b]	Clash (%)[c]	−Den (%)[d]
40.0	1.7	4.8
24.0	14.6	15.6
21.1	19.4	20.9

[a] Three possible fits were found, but the top fit is by far the best.
[b] Sumf, mean density height averaged over all atoms, where the maximum density in the electron density map is set to 100.
[c] Clash, percentage of atoms in the model that approach closer than 5 Å to icosahedral-related capsid protein molecules.
[d] −Den, percentage of atoms in density less than zero density.

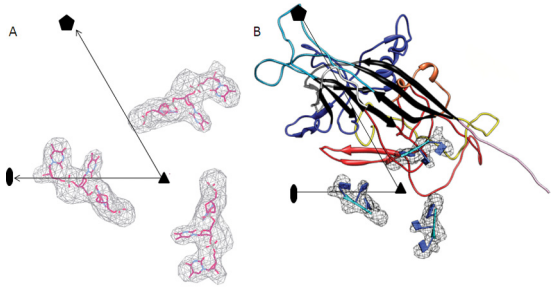

FIG 8 Structure of the three ordered ssDNA bases in *Ad*DNV particles. (A) Difference map between X-ray electron density and cryoEM density, with black lines showing the limits of one icosahedral asymmetric unit. Three bases of the ssDNA were built into the density. (B) Location of the three bases relative to the *Ad*DNV capsid. The colors of the *Ad*DNV capsid polypeptide are as defined for Fig. 1C.

cryoEM. This showed that the heat treatment causes externalization of the N termini while leaving the capsid intact, with the PLA2 domain remaining a part of the particle.

Externalization of the N termini prior to endocytosis abolishes infectivity in parvovirus (53), suggesting that the sequence of events during infection is critical. This could explain why all parvoviruses harbor the N-terminal part of VP1 within the virus particle until they are ready to breach the endosomal membrane. PLA2 requires a Ca^{2+} concentration of greater than 1 mM (9). Such Ca^{2+} concentrations are present in the endosome but not in the cytoplasm (54), further narrowing the viral PLA2 activity to the endosomal membrane.

The 5.5-Å pseudo-atomic-resolution cryoEM structure of emptied *Ad*DNV particles. An initial effort to crystallize heat-treated emptied particles failed to produce crystals, probably because of the externalized VP1 N termini. However, it was possible to obtain a 5.5-Å resolution cryoEM structure from approximately 15,000 images of heat-treated emptied particles (Fig. 5A and B). The structure of the crystallographically determined virus could readily be superimposed onto the cryoEM map by aligning the icosahedral symmetry axes (Table 5). The cryoEM map had to be expanded by 5%, amounting to a radius increase of 6 Å, to obtain the best fit. This change in size of the EM map is well inside the error of determining the magnification of the electron microscope. The quality of the cryoEM map was excellent, as indicated by the resolution of the main chain in some places (Fig. 5E to G).

A 5.5-Å resolution difference map between the crystal structure electron density and the cryoEM map was calculated using the EMfit program (55). This showed two regions of density higher than three standard deviations of the background density, associated with the inside surface of the protein shell. The first region had an average height of about 6.5 σ and could be readily interpreted in terms of three nucleotides (Fig. 8A). This structure was an extended trinucleotide with the bases facing the inside capsid surface (Fig. 8B), close to the icosahedral 3-fold axes with the interaction with Tyr337 and Gln252. The second region had an average height of 3.5 σ but was not easily interpreted in terms of a standard nucleotide structure. Icosahedrally ordered genome structure has been previously observed in canine parvovirus (36) and minute virus of mice (35) but not in invertebrate densoviruses (Table 1).

The density in the channel along the 5-fold axes in the cryoEM map of the emptied particles was similar to that in the crystallographically determined map of the full infectious particle calculated to 5.5-Å resolution (Fig. 5C and D). Thus, the emptied particles still have the glycine-rich region occupying the channel along the 5-fold axes in at least some of the 12 channels of each particle. The externalization of the VP1 termini does not seem to have caused much damage to the particles. In contrast to the case for *Ad*DNV, there is little density along the 5-fold axes of the shrimp (*Pst*DNV) and silkworm (*Bm*DNV) densoviruses. However, these structures are of recombinant particles that contain only VP3 or VP4, respectively, and are therefore missing the glycine-rich region. These observations pose the intriguing question of whether the PLA2 domain has to be refolded to be threaded through the 5-fold pore or whether the pore opens with restoration of the initial capsid structure after extrusion.

ACKNOWLEDGMENTS

We thank Agustin Avila-Sakar and Valorie Bowman for help with the cryo-electron microscopy. We are grateful to Sheryl Kelly for help in preparing the manuscript. We also thank the staff of beamline 23ID, GM/CA-CAT, at Advanced Photon Source, Argonne National Laboratory, for help with the data collection.

Use of the Advanced Photon Source was supported by the U.S. Department of Energy, Office of Science, Office of Basic Energy Sciences, under contract DE-AC02-06CH11357. The work was supported by an NIH grant award (AI11219) to M.G.R. The work was also supported by Purdue University funds for Structural Biology and the Electron Microscope Facility. P.T. was supported by a grant from the Natural Sciences and Engineering Research Council of Canada, and Q.Y. acknowledges tuition waivers at INRS-Institut Armand-Frappier and a scholarship from the People's Republic of China.

G.M., X.Z., P.P, Q.Y., P.T, and M.G.R. designed research; G.M., X.Z., P.P., and Q.Y. performed research; G.M. analyzed data; Q.Y. and P.T. contributed reagents/analytic tools; and G.M., P.T., and M.G.R. wrote the paper.

We declare no conflict of interest.

REFERENCES

1. **Berns K, Parrish CR.** 2006. *Parvoviridae*, p 2437–2478. *In* Knipe DM, Howley PM (ed), Fields virology. Lippincott Williams & Wilkins, Philadelphia, PA.
2. **Bergoin M, Tijssen P.** 2000. Molecular biology of *Densovirinae.* Contrib. Microbiol. **4:**12–32.
3. **Harvell CD, Kim K, Burkholder JM, Colwell RR, Epstein PR, Grimes DJ, Hofmann EE, Lipp EK, Osterhaus AD, Overstreet RM, Porter JW, Smith GW, Vasta GR.** 1999. Emerging marine diseases—climate links and anthropogenic factors. Science **285:**1505–1510.
4. **Li Y, Zadori Z, Bando H, Dubuc R, Fediere G, Szelei J, Tijssen P.** 2001. Genome organization of the densovirus from *Bombyx mori* (*Bm*DNV-1) and enzyme activity of its capsid. J. Gen. Virol. **82:**2821–2825.
5. **Liu K, Li Y, Jousset FX, Zadori Z, Szelei J, Yu Q, Pham HT, Lepine F, Bergoin M, Tijssen P.** 2011. The *Acheta domesticus* densovirus, isolated from the European house cricket, has evolved an expression strategy unique among parvoviruses. J. Virol. **85:**10069–10078.
6. **Szelei J, Woodring J, Goettel MS, Duke G, Jousset FX, Liu KY, Zadori Z, Li Y, Styer E, Boucias DG, Kleespies RG, Bergoin M, Tijssen P.** 2011. Susceptibility of North-American and European crickets to *Acheta domesticus* densovirus (*Ad*DNV) and associated epizootics. J. Invertebr. Pathol. **106:**394–399.
7. **Carlson J, Suchman E, Buchatsky L.** 2006. Densoviruses for control and genetic manipulation of mosquitoes. Adv. Virus Res. **68:**361–392.
8. **Tijssen P.** 1999. Molecular and structural basis of the evolution of parvovirus tropism. Acta Vet. Hung. **47:**379–394.
9. **Canaan S, Zadori Z, Ghomashchi F, Bollinger J, Sadilek M, Moreau ME, Tijssen P, Gelb MH.** 2004. Interfacial enzymology of parvovirus phospholipases A2. J. Biol. Chem. **279:**14502–14508.

10. **Girod A, Wobus CE, Zadori Z, Ried M, Leike K, Tijssen P, Kleinschmidt JA, Hallek M.** 2002. The VP1 capsid protein of adeno-associated virus type 2 is carrying a phospholipase A2 domain required for virus infectivity. J. Gen. Virol. **83:**973–978.
11. **Zadori Z, Szelei J, Lacoste MC, Li Y, Gariepy S, Raymond P, Allaire M, Nabi IR, Tijssen P.** 2001. A viral phospholipase A2 is required for parvovirus infectivity. Dev. Cell **1:**291–302.
12. **Tijssen P, Zadori Z.** April 2002. Viral phospholipase A2 enzymes, antiviral agents and methods of use. WO patent 2,002,000,924.
13. **Farr GA, Zhang LG, Tattersall P.** 2005. Parvoviral virions deploy a capsid-tethered lipolytic enzyme to breach the endosomal membrane during cell entry. Proc. Natl. Acad. Sci. U. S. A. **102:**17148–17153.
14. **Ros C, Gerber M, Kempf C.** 2006. Conformational changes in the VP1-unique region of native human parvovirus B19 lead to exposure of internal sequences that play a role in virus neutralization and infectivity. J. Virol. **80:**12017–12024.
15. **Mani B, Baltzer C, Valle N, Almendral JM, Kempf C, Ros C.** 2006. Low pH-dependent endosomal processing of the incoming parvovirus minute virus of mice virion leads to externalization of the VP1 N-terminal sequence (N-VP1), N-VP2 cleavage, and uncoating of the full-length genome. J. Virol. **80:**1015–1024.
16. **Venkatakrishnan B, Yarbrough J, Domsic J, Bennett A, Bothner B, Kozyreva OG, Samulski RJ, Muzyczka N, McKenna R, Agbandje-McKenna M.** 2013. Structure and dynamics of adeno-associated virus serotype 1 VP1-unique N-terminal domain and its role in capsid trafficking. J. Virol. **87:**4974–4984.
17. **Xie Q, Chapman MS.** 1996. Canine parvovirus capsid structure, analyzed at 2.9 Å resolution. J. Mol. Biol. **264:**497–520.
18. **Agbandje M, McKenna R, Rossmann MG, Strassheim ML, Parrish CR.** 1993. Structure determination of feline panleukopenia virus empty particles. Proteins **16:**155–171.
19. **Simpson AA, Hebert B, Sullivan GM, Parrish CR, Zadori Z, Tijssen P, Rossmann MG.** 2002. The structure of porcine parvovirus: comparison with related viruses. J. Mol. Biol. **315:**1189–1198.
20. **Llamas-Saiz AL, Agbandje-McKenna M, Wikoff WR, Bratton J, Tattersall P, Rossmann MG.** 1997. Structure determination of minute virus of mice. Acta Crystallogr. D Biol. Crystallogr. **53:**93–102.
21. **Halder S, Nam HJ, Govindasamy L, Vogel M, Dinsart C, Salome N, McKenna R, Agbandje-McKenna M.** 2013. Structural characterization of H-1 parvovirus: comparison of infectious virions to empty capsids. J. Virol. **87:**5128–5140.
22. **Kaufmann B, Simpson AA, Rossmann MG.** 2004. The structure of human parvovirus B19. Proc. Natl. Acad. Sci. U. S. A. **101:**11628–11633.
23. **Simpson AA, Chipman PR, Baker TS, Tijssen P, Rossmann MG.** 1998. The structure of an insect parvovirus (*Galleria mellonella* densovirus) at 3.7 Å resolution. Structure **6:**1355–1367.
24. **Kaufmann B, El-Far M, Plevka P, Bowman VD, Li Y, Tijssen P, Rossmann MG.** 2011. Structure of *Bombyx mori* densovirus 1, a silkworm pathogen. J. Virol. **85:**4691–4697.
25. **Kaufmann B, Bowman VD, Li Y, Szelei J, Waddell PJ, Tijssen P, Rossmann MG.** 2010. The structure of *Penaeus stylirostris* densovirus, a shrimp pathogen. J. Virol. **84:**11289–11296.
26. **Xie Q, Bu W, Bhatia S, Hare J, Somasundaram T, Azzi A, Chapman MS.** 2002. The atomic structure of adeno-associated virus (AAV-2), a vector for human gene therapy. Proc. Natl. Acad. Sci. U. S. A. **99:**10405–10410.
27. **Chapman MS, Agbandje-McKenna M.** 2006. Atomic structure of viral particles, p 107–123. *In* Kerr JR, Cotmore S, Bloom ME, Linden RM, Parrish CR (ed), Parvoviruses. Hodder Arnold, London, United Kingdom.
28. **Rossmann MG, Arnold E, Erickson JW, Frankenberger EA, Griffith JP, Hecht HJ, Johnson JE, Kamer G, Luo M, Mosser AG, et al.** 1985. Structure of a human common cold virus and functional relationship to other picornaviruses. Nature **317:**145–153.
29. **Harrison SC, Olson AJ, Schutt CE, Winkler FK, Bricogne G.** 1978. Tomato bushy stunt virus at 2.9 Å resolution. Nature **276:**368–373.
30. **Roberts MM, White JL, Grutter MG, Burnett RM.** 1986. Three-dimensional structure of the adenovirus major coat protein hexon. Science **232:**1148–1151.
31. **Benson SD, Bamford JKH, Bamford DH, Burnett RM.** 1999. Viral evolution revealed by bacteriophage PRD1 and human adenovirus coat protein structures. Cell **98:**825–833.
32. **Nandhagopal N, Simpson AA, Gurnon JR, Yan X, Baker TS, Graves MV, Van Etten JL, Rossmann MG.** 2002. The structure and evolution of the major capsid protein of a large, lipid-containing DNA virus. Proc. Natl. Acad. Sci. U. S. A. **99:**14758–14763.
33. **Bahar MW, Graham SC, Stuart DI, Grimes JM.** 2011. Insights into the evolution of a complex virus from the crystal structure of vaccinia virus D13. Structure **19:**1011–1020.
34. **Xiao C, Kuznetsov YG, Sun S, Hafenstein SL, Kostyuchenko VA, Chipman PR, Suzan-Monti M, Raoult D, McPherson A, Rossmann MG.** 2009. Structural studies of the giant mimivirus. PLoS Biol. **7:**e92. doi:10.1371/journal.pbio.1000092.
35. **Agbandje-McKenna M, Llamas-Saiz AL, Wang F, Tattersall P, Rossmann MG.** 1998. Functional implications of the structure of the murine parvovirus, minute virus of mice. Structure **6:**1369–1381.
36. **Tsao J, Chapman MS, Agbandje M, Keller W, Smith K, Wu H, Luo M, Smith TJ, Rossmann MG, Compans RW, Parrish CR.** 1991. The three-dimensional structure of canine parvovirus and its functional implications. Science **251:**1456–1464.
37. **Chapman MS, Rossmann MG.** 1993. Structure, sequence, and function correlations among parvoviruses. Virology **194:**491–508.
38. **Hogle JM, Chow M, Filman DJ.** 1985. Three-dimensional structure of poliovirus at 2.9 Å resolution. Science **229:**1358–1365.
39. **Otwinowski Z, Minor W.** 1997. Processing of X-ray diffraction data collected in oscillation mode. Methods Enzymol. **276:**307–326.
40. **Tong L, Rossmann MG.** 1997. Rotation function calculations with GLRF program. Methods Enzymol. **276:**594–611.
41. **Rossmann MG.** 1990. The molecular replacement method. Acta Crystallogr. A **46:**73–82.
42. **Kleywegt GJ, Read RJ.** 1997. Not your average density. Structure **5:**1557–1569.
43. **Collaborative Computational Project Number 4.** 1994. The CCP4 suite: programs for protein crystallography. Acta Crystallogr. D Biol. Crystallogr. **50:**760–763.
44. **Emsley P, Cowtan K.** 2004. Coot: model-building tools for molecular graphics. Acta Crystallogr. D Biol. Crystallogr. **60:**2126–2132.
45. **Brünger AT, Adams PD, Clore GM, DeLano WL, Gros P, Grosse-Kunstleve RW, Jiang JS, Kuszewski J, Nilges M, Pannu NS, Read RJ, Rice LM, Simonson T, Warren GL.** 1998. Crystallography and NMR system: a new software suite for macromolecular structure determination. Acta Crystallogr. D Biol. Crystallogr. **54:**905–921.
46. **Ludtke SJ, Baldwin PR, Chiu W.** 1999. EMAN: semiautomated software for high-resolution single-particle reconstructions. J. Struct. Biol. **128:**82–97.
47. **Baker ML, Zhang J, Ludtke SJ, Chiu W.** 2010. Cryo-EM of macromolecular assemblies at near-atomic resolution. Nat. Protoc. **5:**1697–1708.
48. **Scheres SH, Chen S.** 2012. Prevention of overfitting in cryo-EM structure determination. Nat. Methods **9:**853–854.
49. **Higgins DG, Sharp PM.** 1988. CLUSTAL: a package for performing multiple sequence alignment on a microcomputer. Gene **73:**237–244.
50. **Rao ST, Rossmann MG.** 1973. Comparison of super-secondary structures in proteins. J. Mol. Biol. **76:**241–256.
51. **Tamura K, Dudley J, Nei M, Kumar S.** 2007. MEGA4: Molecular Evolutionary Genetics Analysis (MEGA) software version 4.0. Mol. Biol. Evol. **24:**1596–1599.
52. **Garriga D, Pickl-Herk A, Luque D, Wruss J, Caston JR, Blaas D, Verdaguer N.** 2012. Insights into minor group rhinovirus uncoating: the X-ray structure of the HRV2 empty capsid. PLoS Pathog. **8:**e1002473. doi: 10.1371/journal.ppat.1002473.
53. **Boisvert M, Fernandes S, Tijssen P.** 2010. Multiple pathways involved in porcine parvovirus cellular entry and trafficking toward the nucleus. J. Virol. **84:**7782–7792.
54. **Huotari J, Helenius A.** 2011. Endosome maturation. EMBO J. **30:**3481–3500.
55. **Rossmann MG, Bernal R, Pletnev SV.** 2001. Combining electron microscopic with X-ray crystallographic structures. J. Struct. Biol. **136:**190–200.
56. **Wu H, Rossmann MG.** 1993. The canine parvovirus empty capsid structure. J. Mol. Biol. **233:**231–244.